Geophysical Journal International

Geophys. J. Int. (2017) **208,** 177–192
Advance Access publication 2016 September 30
GJI Seismology

doi: 10.1093/gji/ggw370

Upper-mantle velocities below the Scandinavian Mountains from *P*- and *S*-wave traveltime tomography

Babak Hejrani,[1,*] Niels Balling,[1] Bo Holm Jacobsen[1] and Richard England[2]

[1]*Department of Geoscience, Aarhus University, Aarhus, Denmark. E-mail: babak.hejrani@anu.edu.au*
[2]*Department of Geology, University Road, Leicester LE*1 *7RH, United Kingdom*

Accepted 2016 September 29. Received 2016 September 27; in original form 2015 September 27

SUMMARY

The relative traveltime residuals of more than 20 000 arrival times of teleseismic *P* and *S* waves measured over a period of more than 10 yr in five separate temporary and two permanent seismic networks covering the Scandinavian (Scandes) Mountains and adjacent areas of the Baltic Shield are inverted to 3-D tomograms of *P* and *S* velocities and the V_P/V_S ratio. Resolution analysis documents that good 3-D resolution is available under the dense network south of 64° latitude (Southern Scandes Mountains), and patchier, but highly useful resolution is available further north, where station coverage is more uneven. A pronounced upper-mantle velocity boundary (UMVB) that transects the study region is defined. It runs from SE Norway (east of the Oslo Graben) across the mountains to the Norwegian coast near Trondheim (around the Møre–Trøndelag Fault Complex), after which it follows closely along the coast further north. Seismic velocities in the depth interval 100–300 km change significantly across the UMVB from low relative V_P and even lower relative V_S on the western side, to high relative V_P and even higher relative V_S to the east. This main velocity boundary therefore also separates relatively high V_P/V_S ratio to the west and relatively low V_P/V_S to the east. Under the Southern Scandes Mountains (most of southern Norway), we find low relative V_P, even lower relative V_S and hence high V_P/V_S ratios. These velocities are indicative of thinner lithosphere, higher temperature and less depletion and/or fluid content in a relatively shallow asthenosphere. At first sight, this might support the idea of a mantle buoyancy source for the high topography. Under the Northern Scandes Mountains, we find the opposite situation: high relative V_P, even higher relative V_S and hence low V_P/V_S ratios, consistent with thick, dry, depleted lithosphere, similar to that in most of the Baltic Shield area. This demonstrates significant differences in upper-mantle conditions between the Southern and Northern Scandes Mountains, and it shows that upper-mantle velocity anomalies are very poor predictors of topography in this region. An important deviation from this principal pattern is found near the topographic saddle between the Southern and Northern Scandes Mountains. Centred around 64°N, 14°E, a zone of lower *S* velocity and hence higher V_P/V_S ratio is detected in the depth interval between 100 and 300 km. This 'Trøndelag–Jämtland mantle anomaly' (TJMA) is still interpreted as part of relatively undisturbed lithosphere of shield affinity because of high relative *P* velocity, but the relatively low V_P/V_S ratios indicate lower depletion, possibly higher fluid content, and most likely lower viscosity relative to the adjacent shield units. We suggest that this mantle anomaly may have influenced the collapse of the Caledonian Mountains, and in particular guided the location and development of the Møre–Trøndelag Fault Complex. The TJMA is therefore likely to have played an important role in the development of the 'two-dome architecture' of the Scandes Mountains.

Key words: Body waves; Seismic tomography; Cratons; Dynamics of lithosphere and mantle; Europe.

*Now at: Research School of Earth Science, Australian National University, ACT, Australia.

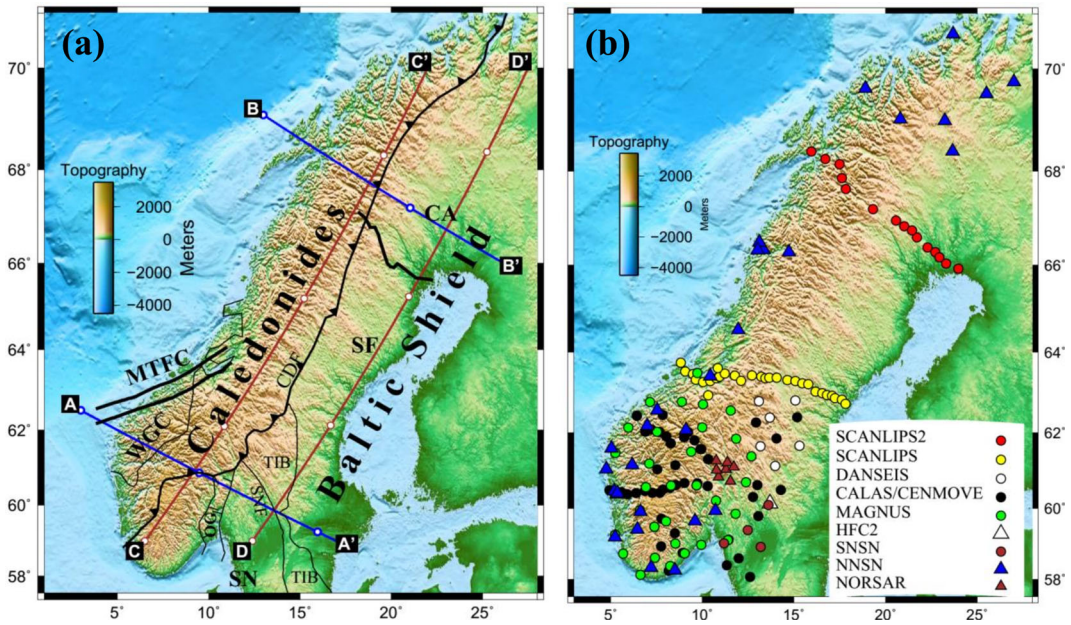

Figure 1. Structural and topographic map of the study area with seismological stations. (a) Structural setting and location of six vertical velocity sections, AA′, BB′, CC′ and DD′. White dots along profiles are indicated at intervals of 200 km. Tectonic abbreviations: CDF, Caledonian Deformation Front; MTFC, Møre–Trøndelag Fault Complex; OG, Oslo Graben; SF, Svecofennian; SN, Sveconorwegian; SNF, Sveconorwegian Front; TIB, Trans-Scandinavian Igneous Belt; WGC, Western Gneiss Complex; CA, Concealed Archean. (b) Triangles show locations of permanent seismological stations, and circles mark stations from different temporary projects, as indicated. Two dense profiles (SCANLIPS, yellow, and SCANLIPS2, red) yield particularly good coverage across the Scandinavian Peninsula. Details of the number of stations for each array/profile with the number of *P*, *SV* and *SH* readings are summarized in Table 1.

1 INTRODUCTION AND TECTONIC OUTLINE

The present study area, which covers the Scandinavian Peninsular, includes two main regional tectonic units—the Scandinavian Caledonides and adjacent parts of the Baltic Shield. It includes the topographically high region of the Scandinavian Mountains, also referred to as the Scandes or Scandes Mountains (Fig. 1a). Deep structural differences in terms of crustal and upper-mantle structure have been reported for these different tectonic and morphologic units; see Ebbing *et al*. (2012) and Maupin *et al*. (2013) for recent results and reviews. Among the main geoscientific issues within this region is the debate concerning the age and origin of high topography for which there is no general consensus (*cf*. Nielsen *et al*. 2009, 2010; Chalmers *et al*. 2010).

The main purpose of this study is to present new high-resolution seismic velocity models (*P*- and *S*-wave velocities) of the upper mantle below the Scandes Mountains and adjacent shield areas. Previous regional studies with comparable resolution covered only the southern part of this study area (Medhus *et al*. 2012a; Wawerzinek *et al*. 2013; Hejrani *et al*. 2015; Kolstrup *et al*. 2015). Regional studies with less station coverage and lower resolution are available and cover larger adjacent areas (e.g. Levshin *et al*. 2007; Jakovlev *et al*. 2012; Zhu *et al*. 2012; Rickers *et al*. 2013). These studies indicate that there may be important differences in the velocity structure of the upper mantle between the Scandes Mountains and the Baltic Shield and also between the two topographic maxima, the Southern Scandes and Northern Scandes Mountains (sometimes referred to as the southern and northern domes, respectively). Such potential differences are of great geodynamic significance. The study area exhibits a general change in the age of the main tectonic units from northeast to southwest and west, with the oldest Archean shield units to the northeast and the youngest, the Scandinavian Caledonides, to the west (Fig. 1a). The central part of the shield is dominated by the 1.9–1.8 Ga Svecofennian Province, bounded to the southwest by the 1.85–1.65 Ga Transscandinavian Igneous Belt. This belt extends for about 1500 km across the Scandinavian Peninsular from southeastern Sweden to northwestern Norway, running in Precambrian crust beneath the Caledonides. The Precambrian units in the southwestern part of the shield were formed about 1.65–1.5 Ga ago, with significant reworking during the 1.15–0.9 Ga old Sveconorwegian orogeny. Precambrian crust in our study area, including the Baltic Shield, constitutes the northwestern part of the palaeocontinent Baltica. For recent studies and reviews of the formation and evolution of this continent, the shield units and its southwestern margins, we refer to Balling (2000), Bogdanova *et al*. (2008), Lahtinen *et al*. (2008) and Bingen *et al*. (2008a,b).

The Scandinavian Caledonides were formed as a result of continent–continent collision between Baltica (with Avalonia) and Laurentia (with Greenland) with the main (Scandian) phase of the orogeny in mid-Silurian to early-Devonian (430–390 Ma, Roberts 2003; Cocks & Torsvik 2006). The Caledonian orogeny, including several earlier phases, generated an extensive mountain range, not only in Scandinavia and eastern Greenland, but extending to the southwest to Scotland, Ireland and North America (*cf*. Cocks & Torsvik 2011). In the present-day North Atlantic region, its original width is estimated to be at least 700–800 km with orogenic remnants that indicate a Himalayan type orogeny (Gee *et al*. 2008). Clear signatures of continent–continent collision are preserved showing pronounced thrust systems, generally east-vergent in Scandinavia and west-vergent in Greenland.

Baltica crust is markedly reworked, in particular to the west in Norwegian coastal areas. In the Western Gneiss Complex (WGC, Fig. 1a), Early Devonian high-pressure rocks, typically eclogites locally bearing coesite and microdiamonds (Dobrzhinetskaya *et al*. 1995), demonstrate subduction of Baltica crust to depths of up to

ca. 125 km. This occurred during the last phase of collision when Laurentia is believed to have been underthrust by Baltica. The orogenic events were followed by gravitational collapse in an extensional tectonic regime (Roberts 2003). Combined with subsequent erosion, this has exposed areas of Precambrian Baltica crust as inliers within the Scandian orogen in various places, including the WGC.

Of special interest are the Scandes Mountains whose topography reaches more than 2000 m in southern and northern areas, but have reduced topography in the central part (Fig. 1). The high topography follows the NE–SW trend of the Caledonides and extends further south and east into the Precambrian shield crust. There is a close negative correlation between surface elevation and Bouguer gravity anomalies. From coastal areas to areas of maximum topography, Bouguer gravity decreases from close to zero to about −100 mGal (Balling 1980; Ebbing *et al*. 2012) with an associated crustal thickness increasing from about 30 km along the coast to around 40 km beneath the crest of the mountains (Svenningsen *et al*. 2007; Stratford *et al*. 2009). This indicates isostatic support for topography, mainly from a thickened crust. The Oslo-Skagerrak area and areas to the south and west of our study region were subject to significant Late Carboniferous-Permian magmatic and tectonic activity (e.g. Heeremans & Faleide 2004). According to Torsvik *et al*. (2008), this magmatism has the characteristics of a Large Igneous Province (LIP) centred on the Skagerrak Sea (Skagerrak-Centred LIP: SCLIP). The Oslo rift and graben system (Fig. 1a), and deep sedimentary basins in the North Sea region, were initiated in relation to these magmatic and tectonic events, with lithospheric stretching in a thermally weakened crust upper mantle acting as an important basin-generating mechanism (Frederiksen *et al*. 2001; McCann *et al*. 2006). During the Mesozoic and Cenozoic, off-shore Norway experienced rifting and subsidence, culminating in the Palaeocene (*ca.* 55 Ma) with the opening of the North Atlantic.

A debate persists concerning the age and origin of the present topography of the Scandes Mountains (*cf*. Nielsen *et al*. 2009, 2010; Chalmers *et al*. 2010). A widely held view has been that the high topography is relatively young, and due to some sort of active tectonic uplift during the Cenozoic (e.g. Dore 1992; Stuevold & Eldholm 1996; Japsen & Chalmers 2000; Lidmar-Bergstrom *et al*. 2000; Gabrielsen *et al*. 2005; Bonow *et al*. 2007; Green *et al*. 2013). Recently, Nielsen *et al*. (2009, 2010) argued that the current topography is mainly a remnant of the Caledonian Mountains. The longevity of topography is here explained by failure of rifting processes to completely destroy the old topography, and to the buoyant, upward-feeding of replacement crustal material commensurate with exhumation unloading. During the Pleistocene, large continental ice sheets covered and depressed the surface of Fennoscandia (Scandinavia and Finland). A number of glaciations have enhanced surface erosion and left a thin cover of glacial materials across low topographic regions. The region is still rebounding today (Balling 1980; Lidberg *et al*. 2010) due to unloading when the thick ice sheet of the last glaciation melted away about 8000–10 000 yr ago.

In this study, we focus on *P*- and *S*-wave velocity variations from relative teleseismic traveltime residuals using a large data set from temporary arrays/profiles and permanent stations in the region across the Scandinavian Caledonides, the Scandes Mountains and the western parts of the Baltic Shield. In particular, we want to test if upper-mantle low-velocity materials may exist beneath areas of high topography in the Northern Scandes Mountains, like those observed in southern Norway. Similarly, we present regional variations in the V_P/V_S ratio. In addition to information on temperature differences as indicated by differences in heat flow between different tectonic units (Balling 1995; Slagstad *et al*. 2009) and by differences in seismic velocities, this ratio is sensitive to compositional variations in the upper mantle. Both types of information are important for the understanding of tectonic and topographic evolution.

2 PREVIOUS STUDIES

Previous studies using data from the Tor Project show the existence of a deep lithosphere boundary close to the Sorgenfrei-Tornquist Zone in southern Sweden—southeastern Denmark (see Gregersen *et al*. 2010, for a summary). Using *P*-wave traveltime residuals and *P*-wave tomography, Medhus *et al*. (2009, 2012a) identified the prolongation of this boundary towards the north into the northern Kattegat—Skagerrak areas and southern Norway. They used data from several projects (MAGNUS, CALAS, CENMOVE, SCANLIPS and Tor, see Fig. 1b), and Wawerzinek *et al*. (2013), applying *S*-wave tomography on MAGNUS data, localized the same main lithosphere boundary in southeast Norway close to the Oslo Graben. Important new information regarding this southern region, containing the Danish and North German Basins and the transition from basins to shield areas across the 'Northern Tornquist Zone', is presented in the independent studies by Hejrani *et al*. (2015) and Kolstrup *et al*. (2015) using combined *P* and *S* tomography, providing also V_P/V_S ratios, similar to this study. *P*-, *SV*- and *SH*-wave upper-mantle velocity structures across the Baltic Shield have been studied using data recorded by the Swedish National Seismological Network (SNSN; Eken *et al*. 2007, 2008). The northeastern part of the shield was studied by the SVEKALAPKO project. The most prominent feature revealed by that study is a high *P*-velocity anomaly which can be followed down to about 250 km beneath the centre of the array (Sandoval *et al*. 2004).

Interesting large regional models for both *P* (Jakovlev *et al*. 2012) and *S* waves (Weidle & Maupin 2008; Zhu *et al*. 2012; Rickers *et al*. 2013) have been published recently suggesting low-velocity upper mantle in southern Norway and an indication of a connection to the northwest into the North Atlantic. This connection is emphasized in particular by Rickers *et al*. (2013), who recover a strong low-velocity region around what they refer to as the 'Iceland Jan Mayen plume system'. The surface-wave study by Levshin *et al*. (2007) mapped *S*-velocity structure in the Barents area as well as the northernmost part of Scandinavia.

3 DATA AND METHODS

Data were combined from permanent arrays (NNSN, NORSAR and SNSN) and several temporary arrays/profiles acquired through international collaboration; CENMOVE (Svenningsen *et al*. 2007), MAGNUS (Weidle *et al*. 2010), CALAS and DANSEIS (Medhus *et al*. 2012a), SCANLIPS (England & Ebbing 2012) and SCANLIPS2 (this paper), see Fig. 1(b) and Table 1. The waveforms recorded at the low-noise broad-band station HFC2 in south-central Sweden (triangle in Fig. 1b) were used as a common reference throughout this project. A common reference station is important since the various arrays were generally not active at the same time.

The *P*- and *S*-arrival-time residuals were determined by the two-step cross-correlation technique presented in Medhus *et al*. (2012a,b), followed by a careful manual check. A total of 21 223 waveforms from 663 events with $M_w > 5.5$ in teleseismic distances (30°–99°) went through the quality control procedure and corrections for ellipticity and crust as described in Hejrani *et al*. 2015, resulting in 12 224 *P* residuals, 3966 *SV* residuals and 4662 *SH* residuals. For details, see Supporting Information S1.

Table 1. Summary information including number of arrival-time readings for seismological stations/arrays applied in this study (compare with Fig. 1b). Temporary arrays are indicated in italic (*cf.* Svenningsen *et al*. 2007; Weidle *et al*. 2010; Medhus *et al*. 2012a; England & Ebbing 2012).

Project/stations	Number of stations	Period of experiment/ recordings	*P*-wave readings	*SV*-wave readings	*ST*-wave readings
SCANLIPS2	15	2007–2009	1358	396	455
SCANLIPS	29	2006–2006	1352	337	361
DANSEIS	6	2008–2009	689	59	73
CALAS/CENMOVE	57	2002–2009	1814	562	576
MAGNUS	34	2006–2008	2334	962	1262
HFC2	1	2002–2012	523	183	205
SNSN	4	2005–2006	56	23	20
NNSN	26	2006–2012	1932	726	886
NORSAR	7	2002–2009	2671	924	960

After these quality-enhancing steps, traveltime residuals were applied in two ways. First, we produced maps of station residuals. At each station, the residuals were computed relative to the reference station HFC2, thus defining the station residual relative to HFC2 for each event. A 'station mean residual' was computed for all individual event residuals at the station. Then, in order to neutralize any bias from the position of HFC2, we subtracted the mean of all 'station mean residuals'.

The resulting relative traveltime station averages (Fig. 2) are generally within ± 1 s for *P*-wave residuals, and, as expected, larger, up to about ± 2 s, for *S* waves.

Finally, the residuals were subjected to traveltime inversions leading to anomaly tomograms of *P*-, *S*-wave velocities and the V_P/V_S ratio, as described below.

Two aspects of the ray distribution require special attention in the parametrization of the velocity models. It is obvious that the stations are distributed differently in the southern and the northern parts of the study area (Fig. 1b). South of the SCANLIPS profile stations are distributed in a rather even and dense pattern, whereas the northern part of the study area is covered by the combination of a relatively sparse, but permanent station array (NNSN), and a dense but temporary profile (SCANLIPS2).

Furthermore, the ray directions are not evenly distributed. Most rays arrive from azimuths between north and east. So, south of the SCANLIPS profile, the ray coverage is good in 3-D, whereas further north, the coverage in 3-D is moderate, except in an inclined zone just under the SCANLIPS2 profile with a very good coverage. We have therefore employed the ray-adaptive technique presented and validated by Hejrani *et al*. (2014). South of SCANLIPS, cells form an approximately Cartesian cubic grid with all sides about 50 km in length. North of SCANLIPS, cells expand and incline progressively so that ray coverage, and hence resolution, is optimized just under the dense SCANLIPS2 profile, as illustrated in Fig. 3. The whole model has been rotated about 35° east, so that it, incidentally, aligns with both the axis of the Scandinavian Peninsula and the main azimuth direction of the rays.

4 RESULTS

4.1 *P*- and *S*-traveltime residuals

The relative *P*- and *S*-traveltime residuals were averaged at each station, as described above. Results shown in Fig. 2 reveal a clear

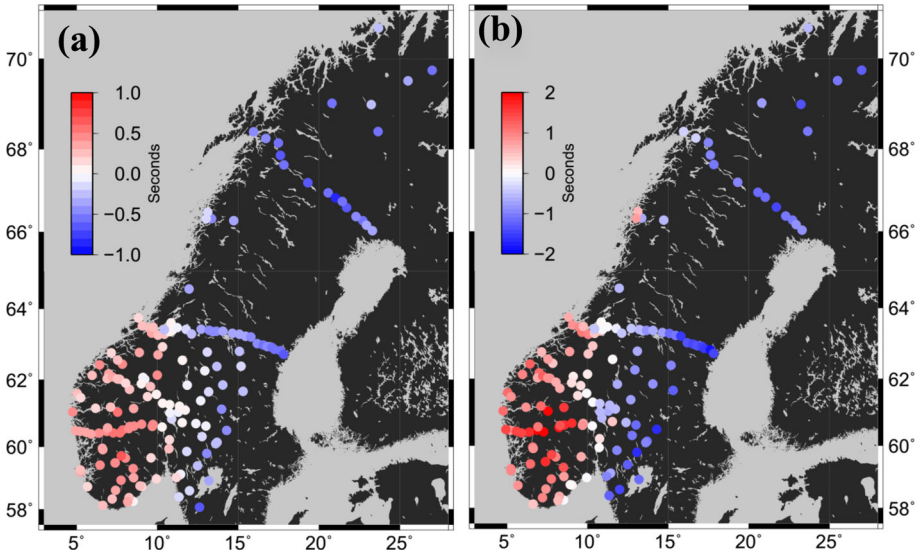

Figure 2. Mean traveltime residual at each seismological station (a) *P* residuals and (b) *S* residuals. A clear first-order east–west transition is seen near the meridian 11°E. Note that this boundary crosses the axis of high topography, which robustly indicates a significant difference between the Southern and Northern Scandes Mountains (*cf.* Fig. 1).

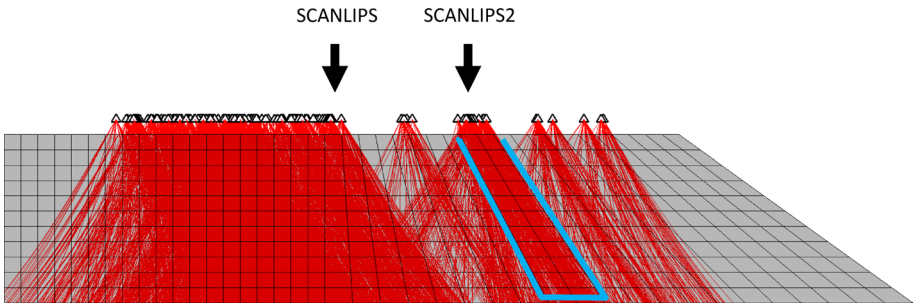

Figure 3. Section through the model along profile CC′ (see Fig. 1), illustrating ray coverage and the principle of the ray-adaptive modelling. Stations and rays are projected onto this profile as seen from southeast. Note the high density of northward and eastward inclined rays coming from the West Pacific Rim. Difference in ray density beneath the southern and the northern parts of the study area requires two different cell patterns. South of the crossing point of the SCANLIPS profile (left arrow) the dense ray coverage calls for traditional 3-D regular cells (50 by 50 by 50 km). North of the SCANLIPS profile the station distribution is sparser. Following Hejrani *et al*. (2014) we adapt the model to the rays as indicated, so that near the crossing point of the SCANLIPS2 profile the model sections follow closely the main ray direction (blue outline). In this way section BB′ in Fig. 7 gets optimized density of crossing rays and hence optimized resolution (see Hejrani *et al*. 2014, for technical details as well as a similar ray-adaptive modelling along the southern SCANLIPS profile).

pattern of relatively late arrivals west of the meridian 11°E, and relatively early arrivals east of this line. Already at this stage we note that for the region as a whole, this trend of traveltime residuals clearly deviates from the structural and topographic trend of the Caledonides and the Scandes Mountains.

4.2 *P*- and *S*-wave tomography

P- and *S*-wave velocity anomalies were computed in the ray-adapted model (Fig. 3) using the tomographic algorithm of Hejrani *et al*. (2014, 2015). See Supporting Information S2 for details on regularization. The resulting *P*-velocity model in Fig. 4 defines model data which fits the observed data with a misfit variance of =0.026 s^2. The total variance of the observed data is 0.087 s^2, so that the variance is reduced by a factor of 3.

The resulting *S*-velocity model in Fig. 5 defines model data which fits the observed data with a misfit variance of $(0.52\ s)^2 = 0.27\ s^2$ which is also three times smaller than the total variance of the observed *S*-data which is 0.84 s^2.

In Figs 4 and 5, cells are blanked if ray coverage is below a threshold, here 112 km which corresponds to ∼2 or more cumulative ray length per cell. This creates an estimated 'unresolved zone' down to ∼200 km between the SCANLIPS and the SCANLIPS2 profiles, except for the coastal areas. In accordance with the station mean residuals of Fig. 2, we find a general boundary, marked out as green dashed lines, with generally lower upper-mantle velocities west of this boundary, and generally higher velocities to the east. To emphasize further details of the pattern of V_P, V_S variations, as well as V_P/V_S variations with depth, four cross-sections (AA′, BB′, CC′, DD′, *cf*. Fig. 1) are outlined. Our discussion of the tomographic results follows below after a resolution analysis.

4.3 V_P/V_S variations

The relative anomalies in the V_P/V_S ratio are calculated from the relative anomalies in V_P and V_S through a simple approximation. For small contrasts, the relative anomaly in V_P/V_S is given by the relative contrast in V_P minus the relative contrast in V_S (see Hejrani *et al*. 2015 for details). Therefore, if V_P and V_S show almost the same contrasts, the V_P/V_S ratio is almost constant and relative variations are close to zero. Hence, the structure in V_P/V_S exposes volumes where V_P and V_S do not vary by the same relative amounts. Our V_P/V_S model is presented in Fig. 6. It shows a distinct contrast of ±1–2 per cent and a pattern resembling those in the *P*- and *S*-velocity tomograms. Our discussion of the finer details in the V_P/V_S ratio follows after the resolution analysis.

4.4 Resolution analysis

The modelling of velocity structure from teleseismic traveltime residuals may, even for ideal station coverage, involve resolution issues. This is even more relevant when station coverage is uneven, as is the case here. The resolution of the recovered *P*- and *S*-wave tomograms has been analysed in two ways. A classical checkerboard test used blocks with a size *ca*. 200 km by *ca*. 200 km by 150 km comparable to that of finer structures seen in the real tomograms. Velocity contrast of ∼3 per cent are separated by a 100 km thick blank zone at a depth of 250–350 km. Blocks thus occupy the depth intervals of 100–250 and 350–500 km, see Fig. 9. Before the inversions we added random noise to the synthetic residuals. Assessment of arrival-time uncertainty led us to a noise level of 0.2 s for the *P* residuals and 0.35 s for the *S* residuals. For details, see Supporting Information S2. The resolution of the checkerboards is seen in Figs 10 and 11. South of latitude ∼65° (close to the SCANLIPS profile), the ray coverage from several arrays/profiles provides good 3-D resolution, and we see very good lateral resolution of checkerboard boundaries, whereas north of 65° latitude the resolution is more patchy, except for volumes around SCANLIPS2. However, the horizontal variations seen in the non-blanked patches actually resolve checkerboard boundaries, such as in the coastal areas near latitude 67°. This is particularly interesting because our main boundary in the real-data tomograms passes this zone (dashed green line in Figs 4–6). Vertical resolution, on the other hand, has intrinsic problems in teleseismic tomography because all rays are relatively steep.

A synthetic structural test examines a simple plausible scenario inspired by the real tomograms. A detailed account of the resolution of V_P, V_S and V_P/V_S in layers from 50 km down to 500 km is found in Supporting Information S3.

Common to these resolution tests, we observe that structures are well resolved but the amplitudes are generally reduced, particularly at deeper levels, sometimes down to less than 50 per cent of the 'real' velocity contrasts in the synthetic model.

5 DISCUSSION AND CONCLUSIONS

Analysis of more than 20 000 waveforms from five separate temporary projects and two permanent networks (from a period of more

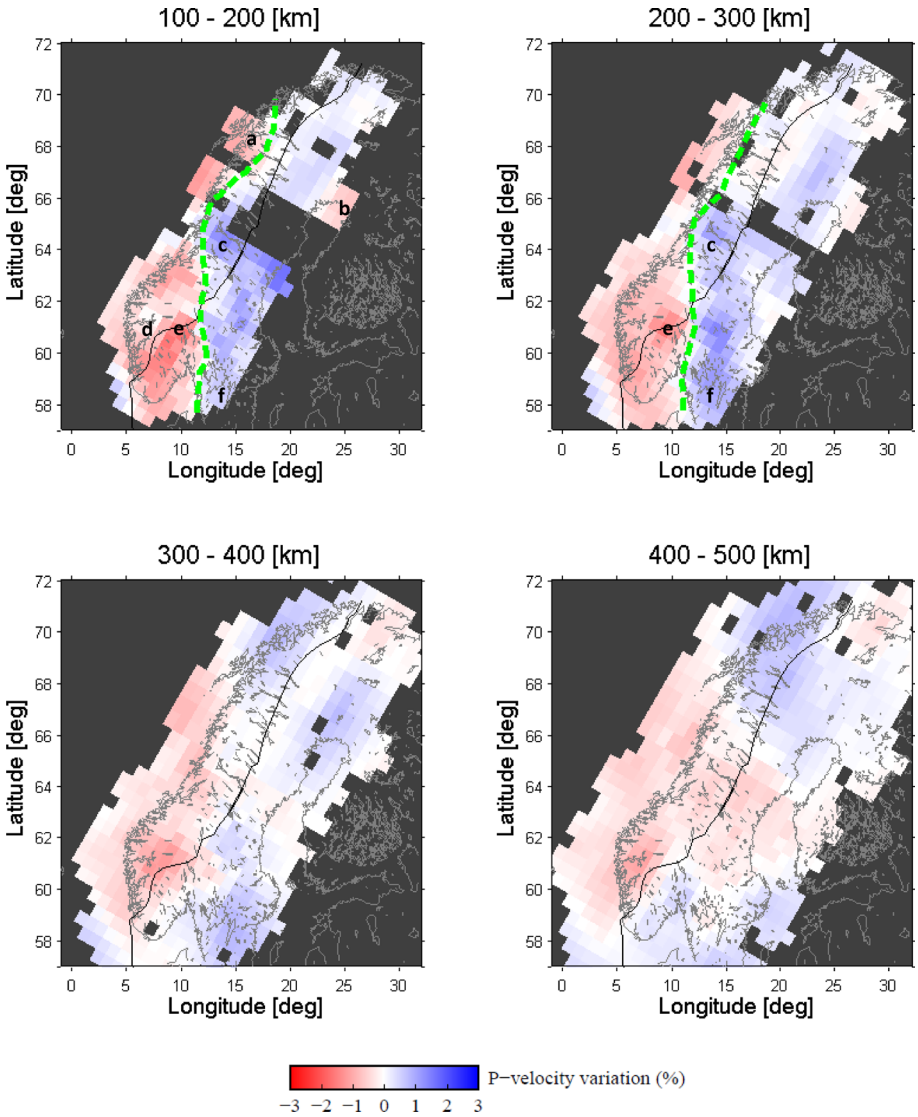

Figure 4. *P*-wave velocity variations in four depth intervals. The black line shows the Caledonian Deformation Front. The dashed green line, shown for the depth intervals of 100–200 and 200–300 km, outlines the main upper-mantle velocity boundary (UMVB). This pronounced boundary continues to the south into the Danish and Danish–Swedish border areas (Medhus *et al*. 2012a; Hejrani *et al*. 2015). Letters indicate localized anomalies, see Table 2.

than 10 yr) covering the Scandes Mountains and adjacent Baltic Shield has revealed clear anomalies in upper-mantle *P*-wave and *S*-wave velocity, as well as the V_P/V_S ratio. As mentioned above, resolution tests show an expected vertical smearing, in particular at the first layer (50–100 km), and the anomaly features are generally recovered at reduced amplitudes. However, the lateral variations are well recovered in the non-blanked areas. The traveltimes were defined from signals with dominant frequencies about 1 Hz for *P* and 0.1 Hz for *S*, which implies a Fresnel-zone-like cross-ray smearing of sensitivity with radius ranging from less than 25 km for *P* waves at mid-lithosphere levels (∼75 km) to about 125 km for *S* waves at the top of the transition zone (∼400 km). The checkerboard in Fig. 9 and the characteristic model in Supporting Information S3 were therefore composed of larger blocks where resolution is not likely to be invalidated by finite-frequency effects. We may therefore proceed to the interpretation of velocity anomalies exposed in the horizontal sections in Figs 4–6 and vertical sections in Figs 7 and 8.

5.1 Main upper-mantle velocity boundary

The main upper-mantle velocity boundary (UMVB) stands out very clearly in the interval 100–300 km in the *P*-velocity model with lower velocities west of the transition and higher velocities to the east (Fig. 4, dashed green curve). *S* velocities (Fig. 5) show the same structure with even larger relative differences. Therefore, the dashed curve also maps a general transition from high V_P/V_S ratios in southern Norway and under the off-shore basins to low V_P/V_S ratios towards the east. An important exception is seen in the Trøndelag–Jämtland area, between latitude 63° and 65°, as discussed below.

The UMVB runs just east of the Oslo Graben and then swings across the Caledonian Deformation Front (Fig. 1a) and the Scandes Mountains in the area of the Møre–Trøndelag Fault Complex (Gabrielsen *et al*. 1999). Previous studies by Medhus *et al*. (2012a), Hejrani *et al*. (2015) and Köhler *et al*. (2015) link this main velocity boundary southwards to the 'lithosphere boundary' mapped by the Tor project (see Gregersen *et al*. 2010 for a review) and

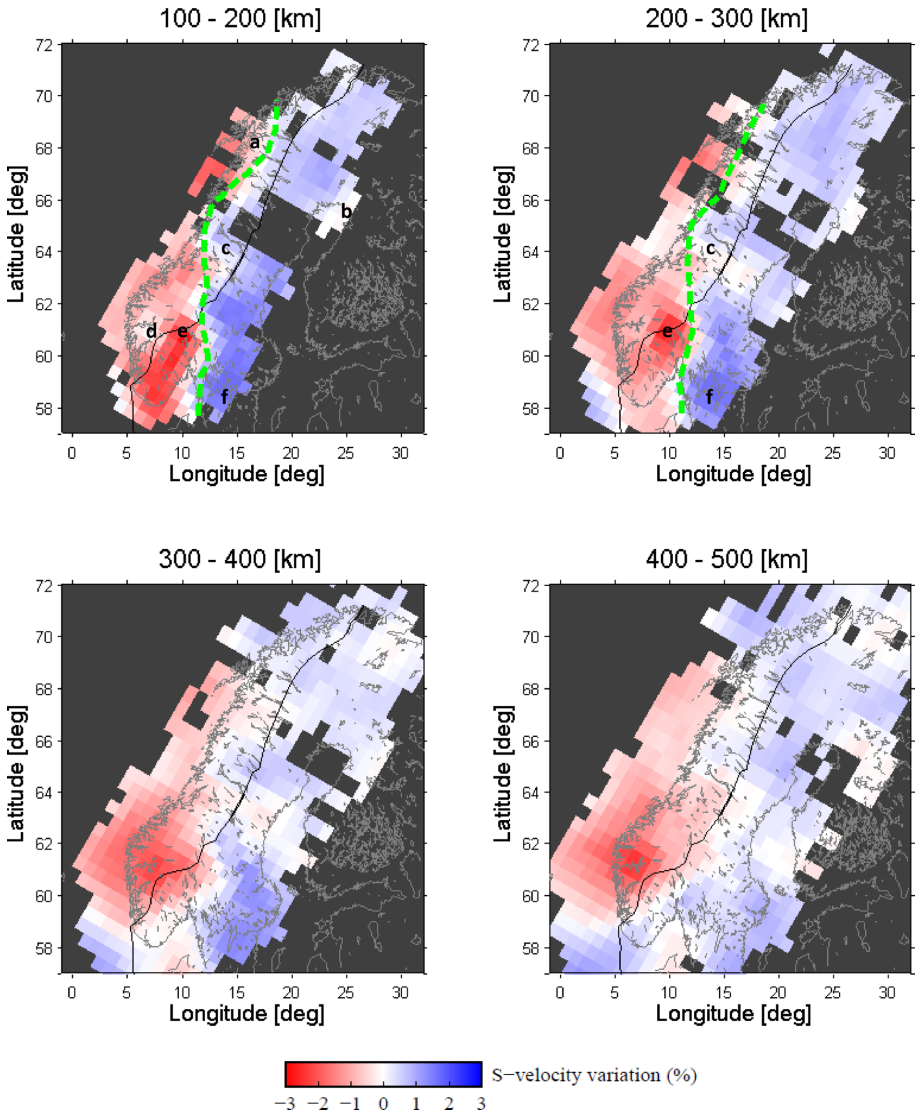

Figure 5. *S*-wave velocity variations at four depth intervals, similar to Fig. 4. The dashed green line, shown for the depth intervals of 100–200 and 200–300 km, is here repeated from Fig. 4 for comparison with the indicated *P*-velocity boundary.

most likely it links up further southwards to a structurally similar UMVB found under the central and southern part of the Tornquist Zone (Zielhuis & Nolet 1994). This study has tracked this mantle velocity boundary northwards where it follows the coast and stays near the western flank of the Scandes Mountains up to latitude 70°N off Lofoten. North of the SCANLIPS array, at about 64°N, the area of resolution narrows. It is clear that the resolution analysis demonstrates that we have very valuable horizontal resolving power, exactly where the UMVB passes close to the coast. Further north the boundary bends inland, associated with what we call the 'Lofoten Slow Spot', centred at 16°E, 68°N (anomaly feature 'a' in Figs 4–6).

We cannot track the UMVB north of 70° with the available land data, but the data coverage does establish that the boundary does not swing inland north of 70°. This conforms very well with the surface-wave study by Levshin *et al.* (2007) where an upper-mantle boundary strikes north under the Barents Sea at about 20° east.

We emphasize that UMVB crosses the axis of the Scandes Mountains, thus demonstrating a significant difference in upper-mantle structure between Southern and Northern Scandes Mountains.

5.2 Localized velocity anomalies

Now we focus on localized velocity anomalies that modify the simple picture with emphasis on *S*-velocity anomalies (Fig. 5). The strongest negative *S* anomaly is found around the northern end of the Oslo Graben. This 'South-eastern Norway Slow Spot' is centred at 10°E, 61°N (anomaly feature 'e' in Figs 4–6; see also Table 2). It has been observed and discussed previously (e.g. Weidle & Maupin 2008; Medhus *et al.* 2012a; Rickers *et al.* 2013; Hejrani *et al.* 2015; Kolstrup *et al.* 2015). On the fast side of the UMVB, we find the large 'South Sweden Fast Zone' centred around 14°E, 58.5°N (anomaly feature 'f', e.g. Medhus *et al.* 2012a; Zhu *et al.* 2012; Hejrani *et al.* 2015). West of the Oslo Graben we find the 'Southwest Norway Fast Spot' (7°E, 61°N, anomaly feature d) which represents a local increase in velocity relative to the general low level on this side of the UMVB. This enigmatic fast spot has come up consistently in previous body-wave tomography studies (e.g. Medhus *et al.* 2012a; Hejrani *et al.* 2015; Kolstrup *et al.* 2015) as well as the surface-wavefield modelling study of Rickers *et al.* (2013). This structure is much smaller and shallower than the South Sweden Fast Zone.

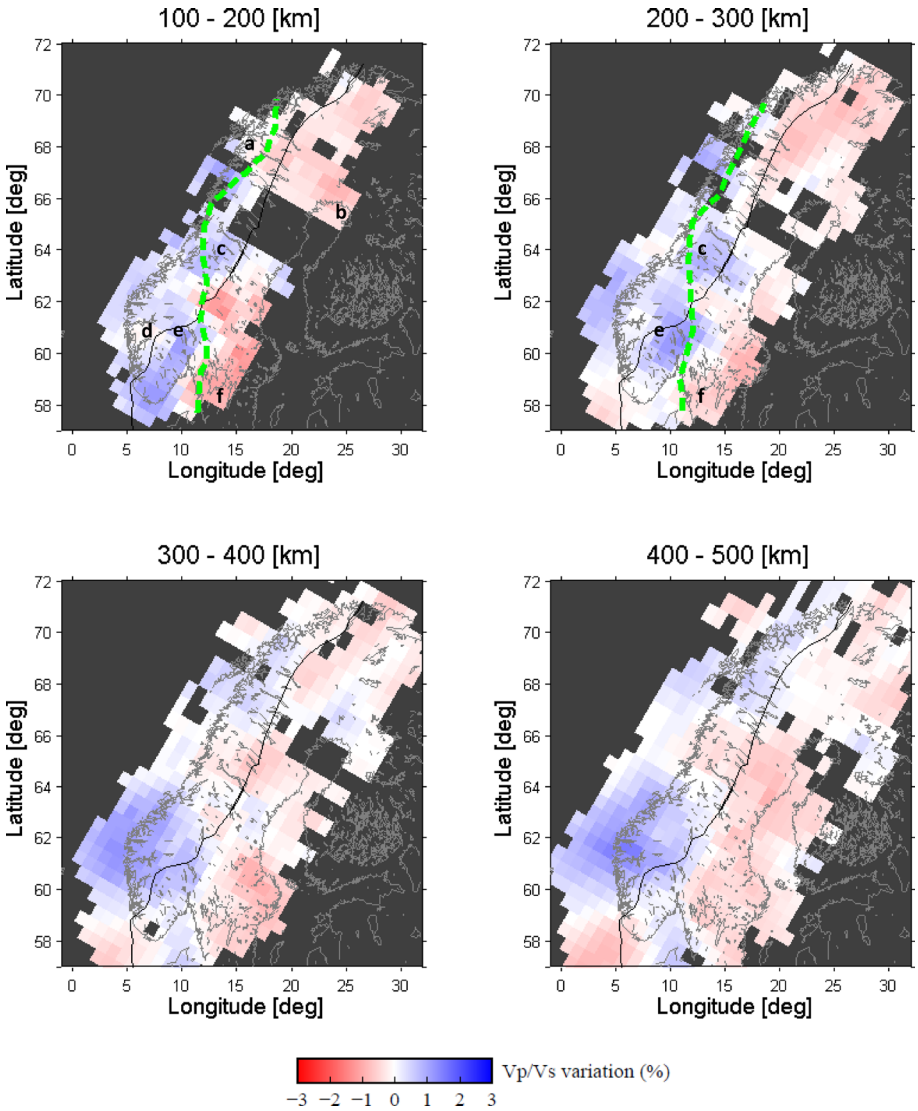

Figure 6. V_P/V_S ratio variations at four depth intervals similar to Figs 4 and 5. The dashed green line, shown for the depth intervals of 100–200 and 200–300 km, is here repeated from Fig. 4 for comparison with the indicated *P*-velocity boundary.

We propose that it is an old lithospheric unit of higher depletion and possibly dryer composition, possibly emplaced together with other units during the Palaeo- and Mesoproterozoic accretion of Southwestern Scandinavia.

The profile section AA′ in Fig. 7, which runs from the Atlantic across the Southern Scandes into Southern Sweden, indicates that this fast spot is relatively shallow, ∼100 km, whereas the UMVB goes deeper, with contrasts in V_P of about ±1 per cent, in V_S of about ±2 per cent and in V_P/V_S ratio of about ±1 per cent. Under the crest of the Southern Scandes Mountains, velocities are generally low, particularly the *S* velocities, and the V_P/V_S ratio is generally high.

The ray-adapted inclined section along the SCANLIPS2 profile (Fig. 7, section BB′), which runs from the Atlantic at Lofoten across the Northern Scandes into Northern Sweden, shows how the Lofoten Slow Spot (anomaly feature 'a') may be a relatively shallow feature (∼100 km). Under the crest of the Northern Scandes Mountains, velocities are generally high, particularly the *S* velocities, and the V_P/V_S ratio is generally low. A low-velocity anomaly is detected at the eastern end of the SCANLIPS2 profile. This North Bothnian Slow Spot (25°E, 65°N, anomaly feature 'b') has also been detected by the SVEKALAPKO project (see Sandoval *et al*. 2004, their fig. 10, levels 150–250 km).

At the eastern boundary of the main UMVB near the saddle of the Scandes Mountains, we find the 'Trøndelag–Jämtland V_P/V_S anomaly' centred at 14°E, 64°N (anomaly feature 'c' in Figs 4–6). The UMVB is traced west of this zone, implied by *P* velocities at the high level typically seen east of the boundary. However, *S* velocities are relatively low, approaching levels found on the western side. Consequently, this high V_P/V_S zone has V_P/V_S ratios typical for the western side of the boundary.

5.3 Influence of temperature and composition on V_P, V_S and V_P/V_S

For the purpose of subsequent discussion, and following Hejrani *et al*. (2015) and Artemieva (2009), we summarize main elements of the effects of temperature and composition upon seismic velocities:

When well below the solidus, that is, in the colder part of lithosphere, a 100 °C temperature rise will reduce both V_P and V_S by about 0.7 per cent (Lee 2003), thus leaving the V_P/V_S ratio

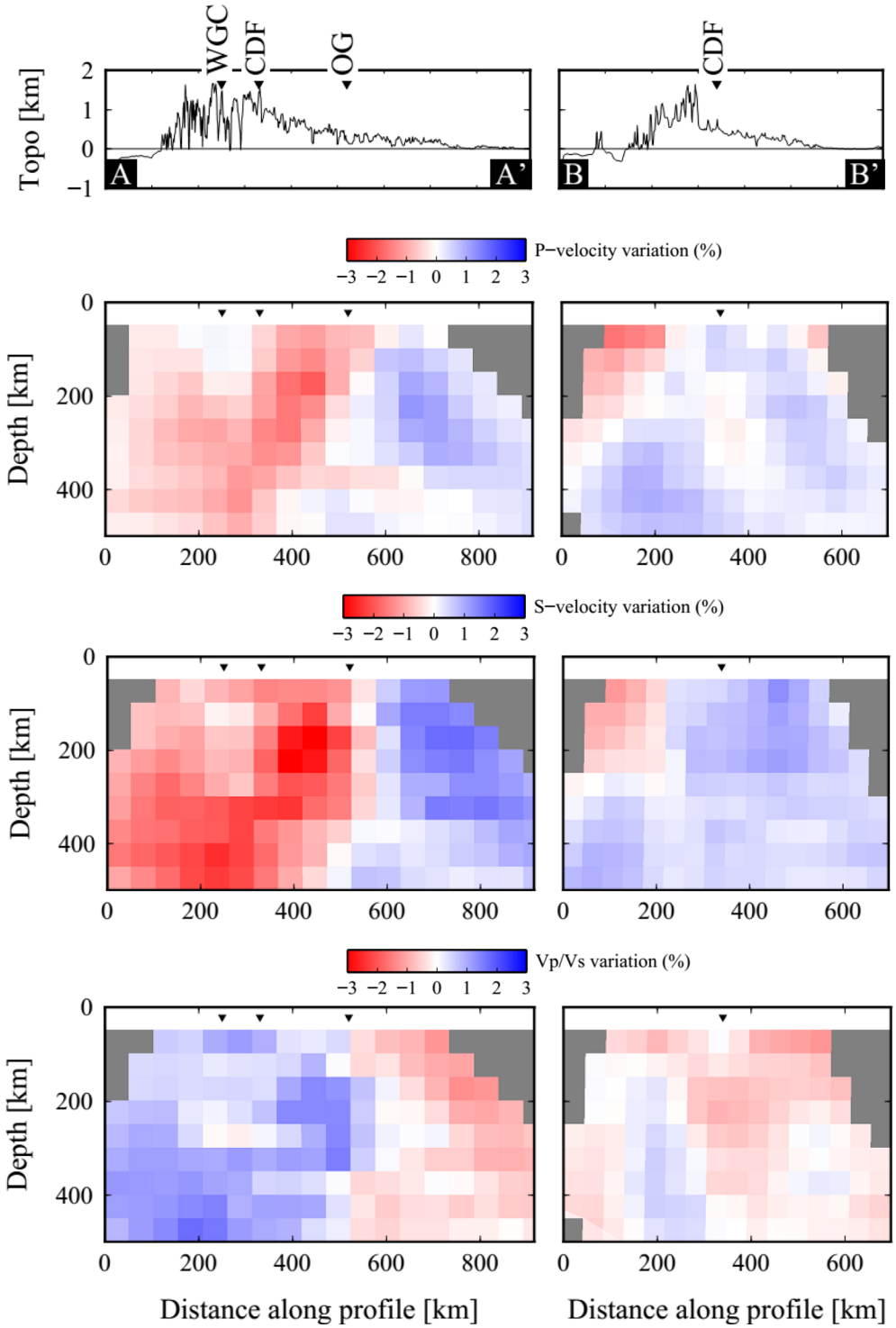

Figure 7. Two NW–SE cross-sections (Fig. 1a) through the *P*-wave, *S*-wave and V_P/V_S models. Section AA′ runs from the southern dome of the Scandes Mountains across the UMVB (upper-mantle velocity boundary) into the Baltic Shield. Section BB′ runs from the Atlantic coast across the UMVB just west of the crest of the northern dome of the Scandes Mountains. The topography and tectonic features along the sections are indicated on the top panel. The topography is exaggerated.

stable. Above the solidus, that is, around the LAB (Lithosphere-Asthenosphere Boundary) and below, the *S* velocity will typically decrease by up to 1–2 per cent per 100 °C (Cammerano *et al*. 2003), thus also making the V_P/V_S ratio somewhat temperature sensitive at larger depths and temperatures. Moreover, possible melts reduce V_S more than V_P, so melts typically increase the V_P/V_S ratio. Traces of water and other fluids will tend to decrease velocities both within the lithosphere and below, and fluids have the added effect of lowering the solidus temperature.

The depletion in iron and other 'basaltic components', as reflected in the magnesium number, Mg# ($100 \times \mathrm{Mg}/(\mathrm{Mg} + \mathrm{Fe})$), will typically raise V_S whereas V_P is largely unaffected (Lee 2003; Schutt &

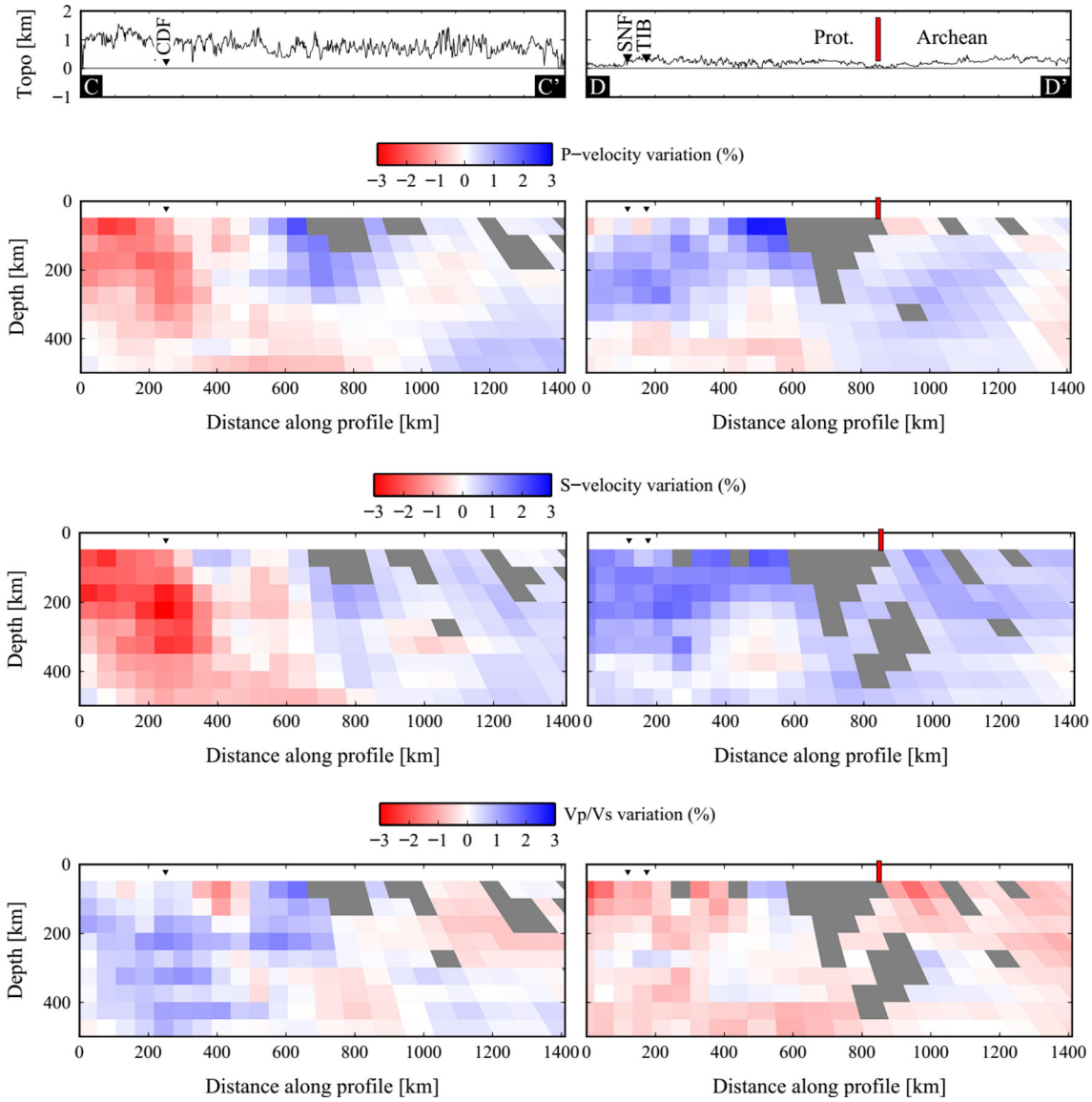

Figure 8. Two SW–NE cross-sections, (Fig. 1a) through the *P*-wave, *S*-wave and V_P/V_S models. Section CC′ runs along the crest of the Scandes Mountains. Note clear velocity difference between the two domes. The parallel section DD′ runs well inside the Proterozoic/Archean units of Baltica. Note the more uniformly high velocities and uniformly negative V_P/V_S under this low-relief shield region. Plots are similar to Fig. 7.

Lesher 2010). Thus large but plausible compositional differences, for example from fertile lherzolite to refractory harzburgite, may imply up to about 1 per cent of increase in V_S and hence 1 per cent decrease in V_P/V_S.

5.4 The history and compositional structure of the main upper-mantle velocity boundary

The high *P* velocities, even higher *S* velocities, and the resulting low V_P/V_S ratios east of the main UMVB are consistent with a very thick, and therefore cold, lithosphere. The low V_P/V_S ratios point towards a composition strongly depleted in Fe and other basaltic components. This interpretation conforms with a number of other studies of the Baltic Shield (*cf.* Artemieva & Thybo 2008 for a recent review), including studies of xenoliths from Finland (Lehtonen *et al.* 2004; Lehtonen & O'Brien 2009). The low *P* velocities and even lower *S* velocities and associated high V_P/V_S ratios west of the UMVB are consistent with a relatively thin, and hence warmer and less depleted lithosphere and a clear asthenosphere low-velocity zone. There is little doubt that the UMVB represents a geologically very significant boundary, although the origin and nature of this boundary varies.

From the Oslo Graben and southwards the UMVB is interpreted as the eastern limit of lithosphere thinning and mantle refertilization associated with the large magmatic events in the Late Carboniferous-Upper Permian that also laid the architecture of the later Danish and North German Basins (Frederiksen *et al.* 2001; Heeremans & Faleide 2004; Medhus *et al.* 2012a; Hejrani *et al.* 2015).

The origin of the UMVB north of the Oslo Graben is less clear. Notably, the boundary runs to the Atlantic coast close to the western boundary of the surface expression of the Trans Scandinavian Igneous Belt (Fig. 1a). Most of southern Norway, including the Southern Scandes Mountains, seems to be underlain by thinner Proterozoic Baltica lithosphere. We interpret the UMVB as the eastern limit of this thinner part of Baltica. Lithosphere

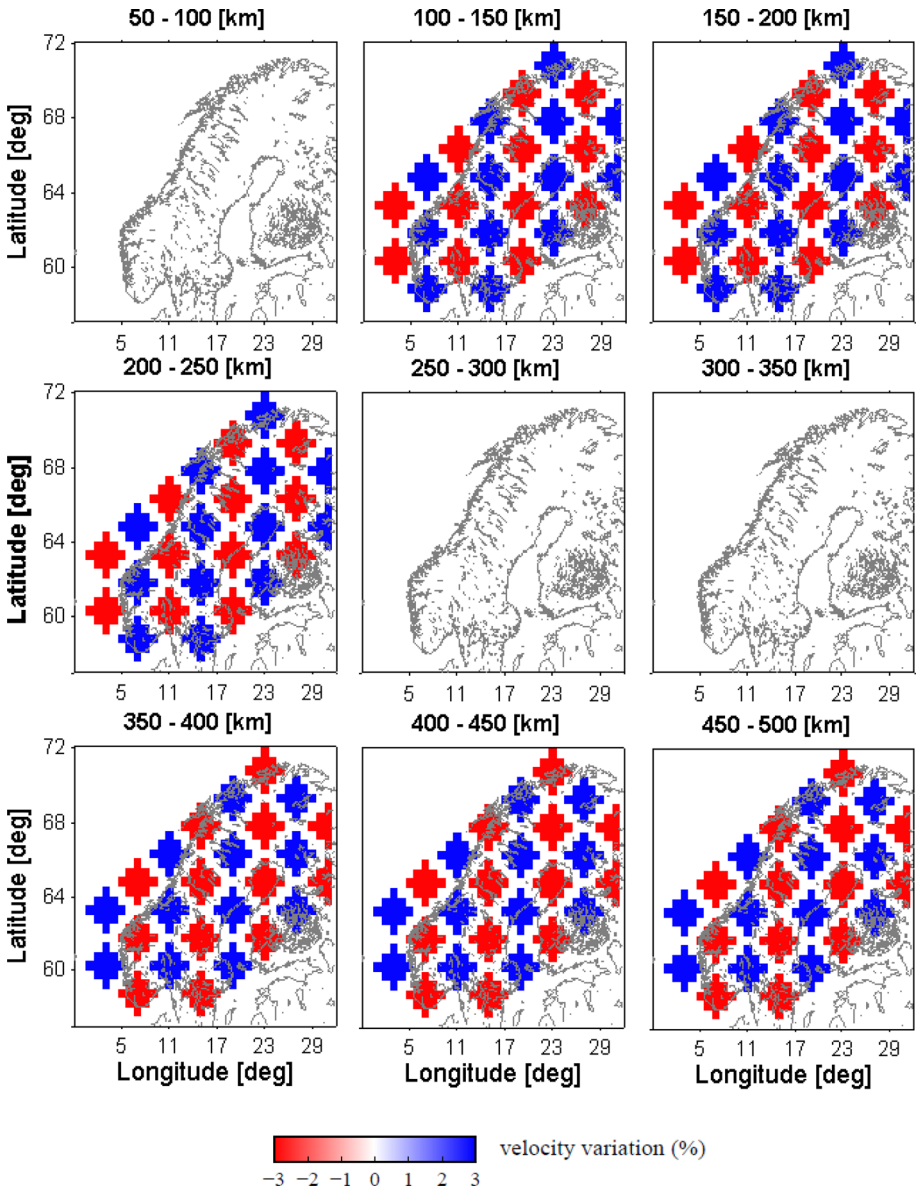

Figure 9. The input checkerboard model, tested for both *P* and *S* waves. Note that, because identical structures and velocity contrasts are applied, the resulting variation in V_P/V_S ratio is constant at zero.

attenuation may originate from several tectonothermal events (Sveconorwegian, Caledonian, Late Carboniferous-Permian and—most recently—Palaeogene opening of the North Atlantic). Even the Pre-Sveconorwegian lithosphere under southern Norway may have been thinner and/or less depleted than the shield areas further east (*cf.* Bingen *et al.* 2008b). Marked compositional differences across the UMVB are supported by a recent integrated geophysical–petrological modelling study by Gradmann *et al.* (2013) who emphasize that differences in the composition of the lithosphere between southern Norway and Sweden are needed to satisfy the gravity field and isostatically compensated topography.

The boundary bends follow the coast at latitude 65°N. Here we interpret this as the eastern limit of several events of rifting and basin formation since the Devonian. Near Lofoten the boundary bends inland associated with the 'Lofoten Slow Spot'. This low-velocity feature is located exactly where the Senja Fracture Zone developed in the Eocene, and is also where the Norwegian coast was closest to the active spreading ridge.

5.5 Trøndelag–Jämtland mantle anomaly

To the east of the main UMVB, centred at 14°E, 64°N, there is a zone of high *P* velocity but with lower *S* velocity and hence higher V_P/V_S ratio (anomaly feature 'c', Figs 6–8). On the basis of these properties, we interpret this zone as uppermost mantle lying within units of shield affinity, but formed of much less depleted mantle than other high V_P units of Baltica. It follows that this 'Trøndelag–Jämtland mantle anomaly' (TJMA) may also have significantly lower viscosity. The high *P*-velocity anomaly is difficult to reconcile with a younger age, so we hypothesize that this mantle anomaly is old and that, in particular, it predates the Caledonian orogeny. It would follow that the creation and collapse of this orogenic belt would be influenced by this viscosity structure around the edge of the colliding Baltica. We therefore suggest that this anomaly may have been a reason for development of the Møre–Trøndelag Fault Complex. This fault complex was mainly active in the Devonian orogenic collapse and in Jurassic rifting, and is an

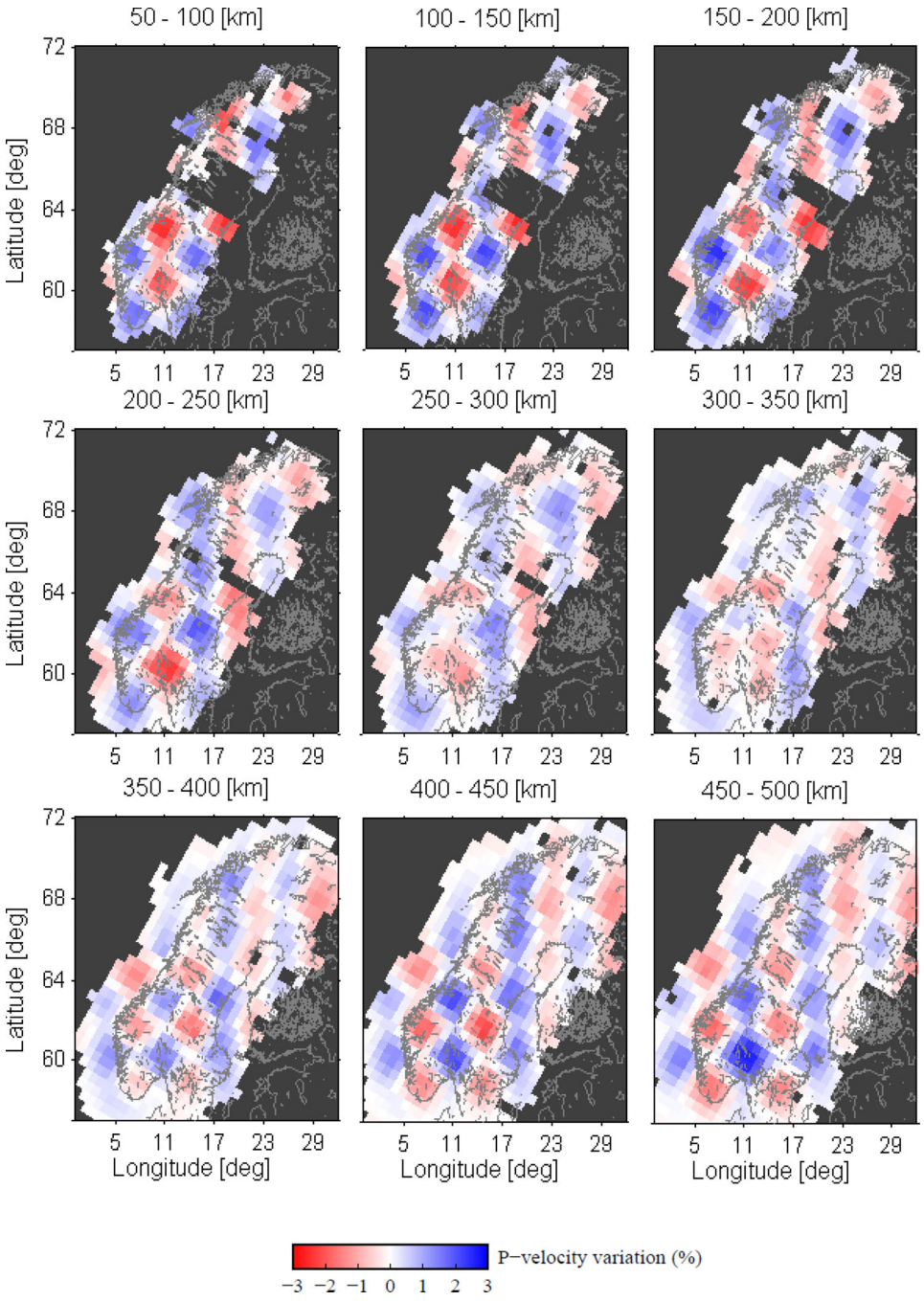

Figure 10. *P*-velocity tomogram recovered for the input checkerboard model shown in Fig. 9. We note that exactly the same ray distribution and regularization is applied here as for the real-data tomogram in Fig. 4. A 0.2 s random noise was added before inversion.

important controlling structure for the development of hydrocarbon-rich basins off-shore (e.g. Gabrielsen *et al*. 1999). The present 'two-dome character' of the Scandes Mountains may be related to the enhanced orogenic collapse and enhanced erosion induced by the Møre–Trøndelag Fault Complex. Thus, the TJMA may have influenced or even pre-conditioned the location of the saddle point of the Scandes Mountains.

5.6 The Scandes Mountains

The question of the source of buoyancy that is presently carrying the prominent, but rather narrow, Scandes Mountains seems largely settled by the good match between the Bouguer gravity anomaly, topography and crustal density structure (*cf*. Ebbing *et al*. 2012). There is little room to accommodate significant subcrustal sources of buoyancy. However, the clear negative shallow mantle anomaly under southern Norway in both *P* and *S* velocity could be viewed as supporting evidence for the hypothesis of dynamic topography and some recent active uplift of the Southern Scandes Mountains (Rickers *et al*. 2013). Figs 7 and 8 focus on this issue. The vertical section AA′ clearly shows the negative anomaly in V_P, the even more negative anomaly in V_S, and the implied positive anomaly in V_P/V_S ratio under southern Norway. The section BB′, which is ray-adapted to the dense profile SCANLIPS2, crosses the

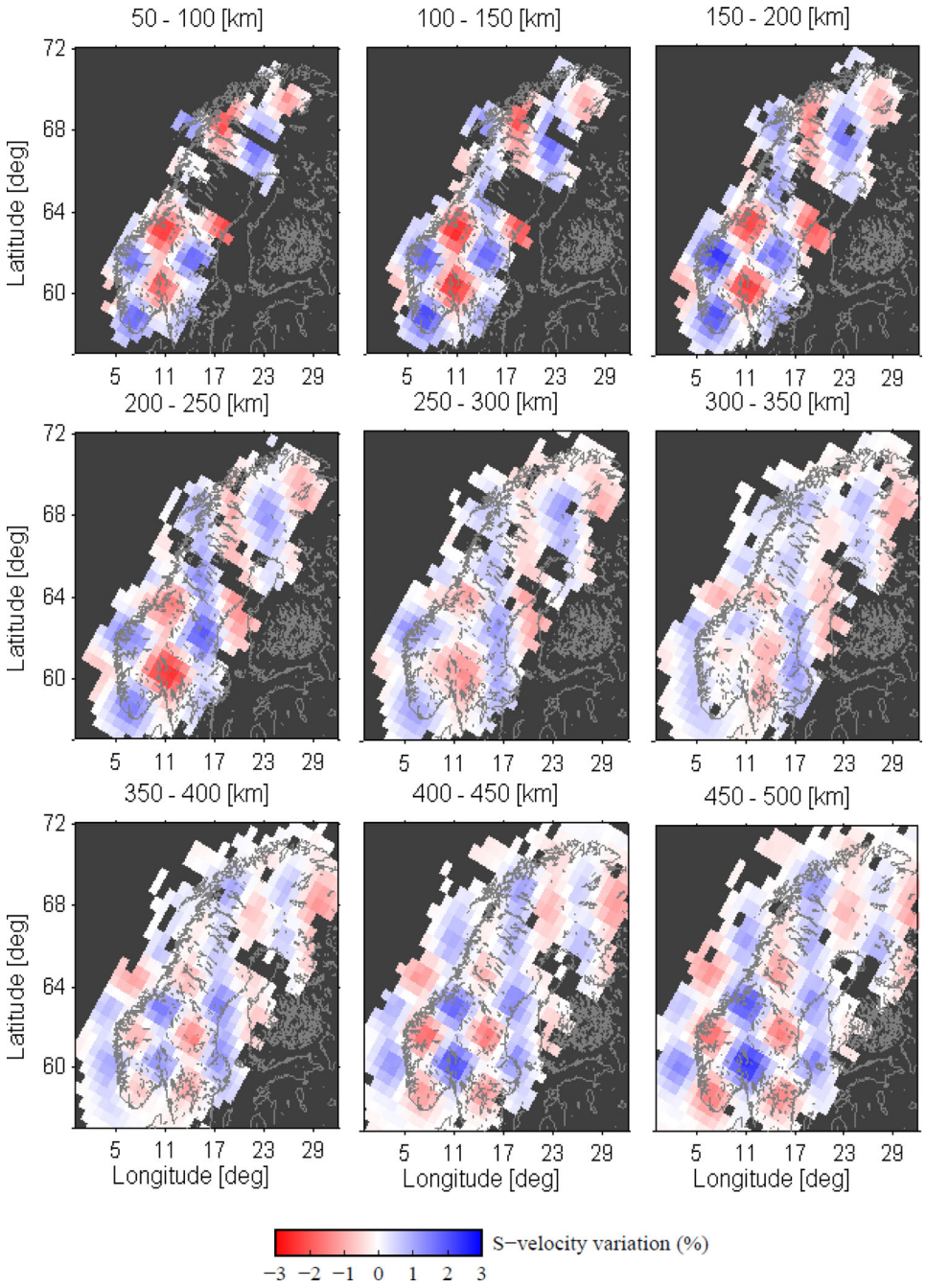

Figure 11. *S*-velocity tomogram recovered for the input checkerboard model shown in Fig. 9. We note that exactly the same ray distribution and regularization is applied here as for the real-data tomogram in Fig. 5. A 0.35 s random noise was added before inversion.

Table 2. Summary of characteristics of main velocity anomaly features with approximate anomaly centres (*cf.* Figs 4–6).

	Longitude	Latitude	Main depth (km)	δV_P (per cent)	δV_S (per cent)	$\delta V_P/V_S$ (per cent)
Main upper-mantle velocity boundary (UMVB)	12°E to 19°E	58°N to 70°N	100–300	±1	±1–2	±1–2
Lofoten Slow Spot, labelled a	16°E	68°N	∼100	−1	−1	∼0
North Bothnian Slow Spot, labelled b	25°E	65°N	100–200	−1	−1	∼0
Trøndelag−Jämtland Mantle Anomaly, labelled c	14°E	64°N	100–300	+1	∼0	+1
Southwest Norway Fast Spot, labelled d	7°E	61°N	100–200	∼0	∼0	∼0
Southeast Norway Slow Spot, labelled e	10°E	61°N	100–300	−2	−3	+1
South Sweden Fast Zone, labelled f	14°E	58.5°N	100–300	+1	+2	−1

Northern Scandes Mountains. Low-velocity levels are only found to the west under the local Lofoten topographic high. In areas of highest topography, we see relatively high V_P and even higher relative V_S, indicating thick, cold, depleted mantle lithosphere. Section CC′ in Fig. 8, which runs along the mountain crest of the Scandes Mountains, shows very clearly the lateral change in mantle velocity from south to north. Section DD′ in Fig. 8 shows the more uniformly high velocities and low V_P/V_S inside the low-relief Baltic Shield. This result clearly weakens the hypothesis of mantle support as the cause of the Scandes Mountains, and hence the hypothesis of dominant uplift in the Neogene loses an otherwise attractive causative mechanism.

However, several tectonothermal events have affected the region of Southern Norway since the Caledonian orogeny. Thus, the Carboniferous-Permian tectonic and magmatic event and the opening of the North Atlantic may have given differential sublithospheric erosion and crustal delamination which may have given subsequent modifications of topography. Moreover, dynamic topography may induce few hundred metres of transient topography as recently analysed by Pedersen *et al*. (2016).

We conclude that significant upper-mantle velocity anomalies exist under the Scandes Mountains. The combination of *P*- and *S*-velocity anomalies to V_P/V_S models greatly enhance the interpretational resolution power of the teleseismic tomography. Thus, when the structures that are detected and delineated by the *P*-and *S*-velocity models are also interpreted by the V_P/V_S ratio, implications for upper-mantle composition and temperature appear.

The main underpinning finding in this study is the northward extension of the pronounced UMVB running across the mountains, thus revealing high upper-mantle seismic velocity under the Northern Scandes Mountains (similar to most of the Baltic Shield area), significantly different from the low-velocity upper mantle below the Southern Scandes. This means that upper-mantle velocity anomalies are very poor predictors of topography in this region.

ACKNOWLEDGEMENTS

This work was conducted in the framework of the TopoScandia-Deep project (part of the ESFTOPO-EUROPE EUROCORES Programme) as well as project TopoReal, both with economic support from the Danish Council for Independent Research. The first author was also supported by a grant from Aarhus University. Acquisition of the SCANLIPS data was supported by the Geological Survey of Norway and equipment loans from the UK Natural Environment Research Council's (NERC) Geophysical Equipment Facility (SEIS-UK). Project MAGNUS data were recorded with the mobile Karlsruhe BroadBand Array (KABBA) of the Karlsruhe Institute of Technology, Germany as well as with permanent stations of the NORSAR array and the Norwegian National Seismological Network (NNSN). Projects CENMOVE and CALAS data were recorded by mobile seismographs from the Geophysical Instrument Pool Potsdam (GIPP), from the UK Natural Environment Research Council's (NERC) Geophysical Equipment Facility (SEIS-UK), from the Danish broad-band pool and from the University of Aarhus. We are grateful to NORSAR (Johannes Schweitzer) and the University of Bergen (Lars Ottemüller) for access to data from permanent stations in Norway, to the University of Uppsala (Roland Roberts), for availability of data from stations of the Swedish SNSN network and to the University of Copenhagen (Hans Thybo) for data from DanSeis stations deployed in Sweden. We acknowledge project coordination by Valerie Maupin, Oslo (TopoScandiaDeep) and Søren B. Nielsen, Aarhus (TopoReal) and are grateful for stimulating discussions. We thank J. Richard Wilson, Aarhus, for improving the English text. Careful reviews by Christian Weidle and Ulrich Achauer led to further important clarifications.

REFERENCES

Artemieva, I.M., 2009. The continental lithosphere: reconciling thermal, seismic, and petrologic data, *Lithos,* **109,** 23–46.

Artemieva, I.M. & Thybo, H., 2008. Deep Norden: highlights of the lithospheric structure of Northern Europe, Iceland, and Greenland, *Episodes,* **31,** 98–106.

Balling, N., 1980. The land uplift in Fennoscandia, gravity field anomalies and isostasy, in *Earth Rheology, Isostasy and Eustasy,* pp. 297–321, ed. Morner, N.-A., John Wiley & Sons.

Balling, N., 1995. Heat flow and thermal structure of the lithosphere across the Baltic Shield and northern Tornquist Zone, *Tectonophysics,* **244,** 13–50.

Balling, N., 2000. Deep seismic reflection evidence for ancient subduction and collision zones within the continental lithosphere of northwestern Europe, *Tectonophysics,* **329,** 269–300.

Bingen, B., Andersson, J., Söderlund, U. & Möller, C., 2008a. The Mesoproterozoic in the Nordic countries, *Episodes,* **31,** 29–34.

Bingen, B., Nordgulen, Ø. & Viola, G., 2008b. A four-phase model for the Sveconorwegian orogeny, SW Scandinavia, *Norw. J. Geol.,* **88,** 43–72.

Bogdanova, S.V., Bingen, B., Gorbatschev, R., Kheraskova, T.N., Kozlov, V.I., Puchkov, V.N. & Volozh, Yu.A., 2008. The East European Craton (Baltica) before and during the assembly of Rodinia, *Precambrian Res.,* **160,** 23–45.

Bonow, J.M., Lidmar-Bergstrom, K., Japsen, P., Chalmers, J.A. & Green, P.F., 2007. Elevated erosion surfaces in central West Greenland and southern Norway: their significance in integrated studies of passive margin development, *Norw. J. Geol.,* **87,** 197–206.

Cammerano, F., Goes, S., Vacher, P. & Giardini, D., 2003. Inferring upper mantle temperatures from seismic velocities, *Phys. Earth planet. Inter.,* **138,** 197–222.

Chalmers, J.A., Green, P., Japsen, P. & Rasmussen, E.S., 2010. The Scandinavian mountains have not persisted since the Caledonian orogeny. A comment on Nielsen *et al*. (2009a), *J. Geodyn.,* **50,** 94–101.

Cocks, L.R.M. & Torsvik, T.H., 2006. European geography in a global context from the Vendian to the end of the Palaeozoic, in *European Lithosphere Dynamics,* Vol. 32, pp. 83–95, eds Gee, D.G. & Stephenson, R.A., Geol. Soc. London Mem.

Cocks, L.R.M. & Torsvik, T.H., 2011. The Palaeozoic geography of Laurentia and western Laurussia: a stable craton with mobile margins, *Earth-Sci. Rev.,* **106,** 1–51.

Dobrzhinetskaya, L.F., Eide, E.A., Larsen, R.B., Smith, D.C., Sturt, B.A., Tronnes, R.G., Taylor, W.R. & Poshukhova, T.V., 1995. Microdiamonds in high-grade metamorphic rocks from the Western Gniess Region, Norway, *Geology,* **23,** 597–600.

Dore, G.A., 1992. The base Tertiary surface of southern Norway and the northern North Sea, *Norw. J. Geol.,* **72,** 259–265.

Ebbing, J., England, R.W., Korja, T., Lauritsen, T., Olesen, O., Stratford, W. & Weidle, C., 2012. Structure of the Scandes lithosphere from surface to depth, *Tectonophysics,* **536,** 1–24.

Eken, T., Shomali, H., Roberts, R. & Bodvarsson, R., 2007. Upper-mantle structure of the Baltic Shield below the Swedish National Seismological Network (SNSN) resolved by teleseismic tomography, *Geophys. J. Int.,* **169,** 617–630.

Eken, T., Shomali, H., Roberts, R., Hieronymus, C.F. & Bodvarsson, R., 2008. S and P velocity heterogeneities within the upper mantle below the Baltic Shield, *Tectonophysics,* **462,** 109–124.

England, R.W. & Ebbing, J., 2012. Crustal structure of central Norway and Sweden from integrated modelling of teleseismic receiver functions and the gravity anomaly, *Geophys. J. Int.,* **191,** 1–11.

Frederiksen, S., Nielsen, S.B. & Balling, N., 2001. A numerical dynamic model for the Norwegian-Danish Basin, *Tectonophysics,* **343,** 165–183.

Gabrielsen, R.H., Braathen, A., Olesen, O., Faleide, J.I., Kyrkjebø, R. & Redfield, T., 2005. Vertical movements in south-western Fennoscandia: a discussion of regions and processes from the present to the Devonian, in *Onshore–Offshore Relationships on the North Atlantic Margin,* Vol. 12, pp. 1–28, eds Wandås, B., Eide, E., Grandstein, F. & Nystuen, J., Norwegian Petroleum Society (NPF) Special Publication, Elsevier.

Gabrielsen, R.H., Odinsen, T. & Grunnaleite, I., 1999. Structuring of the northern Viking graben and the Møre basin; the influence of basement structural grain and the particular role of the Møre-Trøndelag fault complex, *Mar. Petrol. Geol.,* **16,** 443–465.

Gee, D.G., Fossen, H., Henriksen, N. & Higgins, A.K., 2008. From the early Paleozoic platforms of Baltica and Laurentia to the Caledonide Orogen of Scandinavia and Greenland, *Episodes,* **31,** 44–51.

Gradmann, S., Ebbing, J. & Fullea, J., 2013. Integrated geophysical modelling of a lateral transition zone in the lithospheric mantle under Norway and Sweden, *Geophys. J. Int.,* **194,** 1358–1373.

Green, P.F., Lidmar-Bergström, K., Japsen, P., Bonow, J.M. & Chalmers, J.A., 2013. Stratigraphic landscape analysis, thermochronology and the episodic development of elevated, passive continental margins, in *Geological Survey of Denmark and Greenland Bulletin,* Vol. 30, 150 pp., Danish Ministry of Climate, Energy and Building.

Gregersen, S., Voss, P., Nielsen, L.V., Achauer, U., Busche, H., Rabbel, W. & Shomali, Z.H., 2010. Uniqueness of modeling results from teleseismic *P*-wave tomography in Project Tor, *Tectonophysics,* **481,** 1–4.

Heeremans, M. & Faleide, J.I., 2004. Late Carboniferous-Permian tectonics and magmatic activity in the Skagerrak, Kattegat and North Sea, in *Permo-Carboniferous Magmatism and Rifting in Europe,* pp. 157–179, eds Wilson, M., Neumann, E.R., Davies, G.R., Timmerman, M.J., Heeremans, M. & Larsen, B.T., Vol. 233, Geol. Soc. London, Spec. Publ.

Hejrani, B., Balling, N., Jacobsen, B.H. & Tilmann, F., 2015. Upper-mantle *P*- and *S*-wave velocities across the Northern Tornquist Zone from traveltime tomography, *Geophys. J. Int.,* **203,** 437–458.

Hejrani, B., Jacobsen, B.H. & Balling, N., 2014. Teleseismic tomography when stations follow profiles: pitfalls and remedies, *Seismol. Res. Lett.,* **85,** 997–1003.

Jakovlev, A., Bushenkova, N.A., Koulakov, I.Y. & Dobretsov, N.L., 2012. Structure of the upper mantle in the Circum-Arctic region from regional seismic tomography, *Russ. Geol. Geophys.,* **53,** 963–971.

Japsen, P. & Chalmers, J.A., 2000. Neogene uplift and tectonics around the north Atlantic: overview, *Global Planet. Change,* **24,** 165–173.

Köhler, A., Maupin, V. & Balling, N., 2015. Surface wave tomography across the Sorgenfrei- Tornquist Zone, SW Scandinavia, using ambient noise and earthquake data, *Geophys. J. Int.,* **203,** 284–311.

Kolstrup, M., Hung, S.-H. & Maupin, V., 2015. Multiscale, finite-frequency P and S tomography of the upper mantle in the southwestern Fennoscandian Shield, *Geophys. J. Int.,* **202,** 190–218.

Lahtinen, R., Garde, A.A. & Melezhik, V.A., 2008. Paleoproterozoic evolution of Fennoscandia and Greenland, *Episodes,* **31,** 20–28.

Lee, C.-T.A., 2003. Compositional variation of density and seismic velocities in natural peridotites at STP conditions: implications for seismic imaging of compositional heterogeneities in the upper mantle, *J. geophys. Res.,* **108,** 2441, doi:10.1029/2003JB002413.

Lehtonen, M. & O'Brien, H., 2009. Mantle transect of the Karelian Craton from margin to core based on *P-T* data from garnet and clinopyroxene xenocrysts in kimberlites, *Bull. geol. Soc. Finland,* **81,** 79–102.

Lehtonen, M., O'Brien, H., Peltonen, P., Johanson, B. & Pakkanen, L., 2004. Layered mantle at the Karelian Craton margin: *P-T* of mantle xenocrysts and xenoliths from the Kaavi-Kuopio kimberlites, Finland, *Lithos,* **77,** 593–608.

Levshin, A.L., Schweitzer, J., Weidle, C., Shapiro, N.M. & Ritzwoller, M.H., 2007. Surface wave tomography of the Barents Sea and surrounding regions, *Geophys. J. Int.,* **170,** 441–459.

Lidberg, M., Johansson, J.M., Scherneck, H.-G. & Milne, G.A., 2010. Recent results based on continuous GPS observations of the GIA process in Fennoscandia from BIFROST, *J. Geodyn.,* **50,** 8–18.

Lidmar-Bergstrom, K., Ollier, C.D. & Sulebak, J.R., 2000. Landforms and uplift history of southern Norway, *Global Planet. Change,* **24,** 211–231.

Maupin, V. *et al.*, 2013. The deep structure of the Scandes and its relation to tectonic history and present-day topography, *Tectonophysics,* **602,** 15–37.

McCann, T. *et al.*, 2006. Post-Variscan (end Carboniferous-Early Permian), basin evolution in Western and Central Europe, in *European Lithosphere Dynamics,* Vol. 32, pp. 355–388, eds Gee, D.G. & Stephenson, R.A., Geol. Soc. London Mem.

Medhus, A.B., Balling, N., Jacobsen, B.H., Kind, R. & England, R.W., 2009. Deep-structural differences in southwestern Scandinavia revealed by *P*-wave travel time residual, *Norw. J. Geol.,* **89,** 203–214.

Medhus, A.B., Balling, N.B., Jacobsen, B.H., Weidle, C., England, R.W., Kind, R., Thybo, H. & Voss, P., 2012a. Upper-mantle structure beneath the Southern Scandes Mountains and the Northern Tornquist Zone revealed by *P*-wave traveltime tomography, *Geophys. J. Int.,* **189,** 1315–1334.

Medhus, A.B., Jacobsen, B.H. & Balling, N., 2012b. Bias problems in existing teleseismic travel time databases: ignore or repair?, *Seism. Res. Let.,* **83**(6), 1030–1037.

Nielsen, S.B., Clausen, O.R., Jacobsen, B.H., Thomsen, E., Huuse, M., Gallagher, K., Balling, N. & Egholm, D.L., 2010. The ICE hypothesis stands: how the dogma of late Cenozoic tectonic uplift can no longer be sustained in the light of data and physical laws, *J. Geodyn.,* **50,** 102–111.

Nielsen, S.B. *et al.*, 2009. The evolution of western Scandinavian topography: a review of Neogene uplift versus the ICE (isostasy-climate-erosion) hypothesis, *J. Geodyn.,* **47,** 72–95.

Pedersen, V.K., Huismans, R.S. & Moucha, R., 2016. Isostatic and dynamic support of high topography on a North Atlantic passive margin, *Earth planet. Sci. Lett.,* **446,** 1–9.

Rickers, F., Fichtner, A. & Trampert, J., 2013. The Iceland-Jan Mayen plume system and its impact on mantle dynamics in the North Atlantic region: evidence from full-waveform inversion, *Earth planet. Sci. Lett.,* **367,** 39–51.

Roberts, D., 2003. The Scandinavian Caledonides: event chronology, palaeogeographic setting and likely modern analogues, *Tectonophysics,* **365,** 283–299.

Sandoval, S., Kissling, E. & Ansorge, J. & SVEKALAPKO Seismic Tomography Working Group, 2004. High-resolution body wave tomography beneath the SVEKALAPKO array—II. Anomalous upper mantle structure beneath the central Baltic Shield, *Geophys. J. Int.,* **157,** 200–214.

Schutt, D.L. & Lesher, C.E., 2010. Compositional trends among Kaapvaal Craton garnet peridotite xenoliths and their effects on seismic velocity and density, *Earth planet. Sci. Lett.,* **300,** 367–373.

Slagstad, T., Balling, N., Elvebakk, H., Midttømme, K., Olesen, O., Olsen, L. & Pascal, C., 2009. Heat-flow measurements in Late Palaeoproterozoic to Permian geological provinces in south and central Norway and a new heat-flow map of Fennoscandia and the Norwegian-Grenland Sea, *Tectonophysics,* **473,** 341–361.

Stratford, W., Thybo, H., Faleide, J.I., Olesen, O. & Tryggvason, A., 2009. New Moho Map for onshore southern Norway, *Geophys. J. Int.,* **178,** 1755–1765.

Stuevold, L.M. & Eldholm, O., 1996. Cenozoic uplift of Fennoscandia inferred from a study of the mid-Norwegian margin, *Global Planet. Change,* **12,** 359–386.

Svenningsen, L., Balling, N., Jacobsen, B.H., Kind, R., Wylegalla, K. & Schweitzer, J., 2007. Crustal root beneath the highlands of southern Norway resolved by teleseismic receiver functions, *Geophys. J. Int.,* **170,** 1129–1138.

Torsvik, T.H., Smethurst, M.A., Bruke, K. & Steinberger, B., 2008. Long term stability in deep mantle structure: evidence from the ∼300 Ma Skagerrak-Centered Large Igneous Province (the SCLIP), *Earth planet. Sci. Lett.,* **267,** 444–452.

Wawerzinek, B., Ritter, J.R.R. & Roy, C., 2013. New constraints on the 3-D shear wave velocity structure of the upper mantle underneath Southern Scandinavia revealed from non-linear tomography, *Tectonophysics,* **602,** 38–54.

Weidle, C. *et al.*, 2010. MAGNUS—a seismological broadband experiment to resolve crustal and upper mantle structure beneath the Southern Scandes Mountains in Norway, *Seismol. Res. Lett.,* **81,** 76–84.

Weidle, C. & Maupin, V., 2008. An upper-mantle *S*-wave velocity model for Northern Europe from Love and Rayleigh group velocities, *Geophys. J. Int.,* **175,** 1154–1168.

Zhu, H., Bozdağ, E., Peter, D. & Tromp, J., 2012. Structure of the European upper mantle revealed by adjoint tomography, *Nat. Geosci.,* **5,** 493–498.

Zielhuis, A. & Nolet, G., 1994. Deep seismic expression of an ancient plate boundary in Europe, *Science,* **265,** 79–81.

SUPPORTING INFORMATION

Additional Supporting Information may be found in the online version of this paper:

S1: Details on data processing and quality control

Figure S1-1. Example illustrating the picking process for an *SH* wave on the T component (event 2011 March 09 02:45:20 M_w 7.3). Waveforms are filtered using a 'mixed-filter' (Medhus *et al*. 2012b) at 0.05–0.2 Hz. Station HFC2 is selected as the reference station (black waveform). (a) Raw waveforms before removing the instrument response. (b) Results of cross-correlation (grey waveforms) using instrument-corrected waveforms. We see a significant improvement in waveform similarity between the broad-band reference station (HFC2) and short-period stations like HYA, KTK1 and SNART. Picks are shown with green dots on each waveform. The residual at HAMF is an example of an outlier which is removed automatically by the two criteria: all residuals must be less than 5 s from the residual at HFC2 and less than 3 s from the median for the event.

Figure S1-2. Location of the seismological events used in this study. The yellow frame shows the study area.

S2: Details on tomographic inversion

S3: Additional resolution analysis

Figure S3-1. Synthetic characteristic input model, inspired by the real-data model. This test resembles a plausible mix of thick homogenous 'fast' lithospheric blocks beneath the Baltic Shield and 'slow volumes' beneath southern Norway and along the coastal area of northern Norway. Again, identical structures and the same relative velocity contrasts are applied for *P* and *S* modelling, resulting in a constant V_P/V_S ratio.

Figure S3-2. *P*-velocity tomogram recovered for the input block model shown in Fig. S3-1, again using exactly the same ray distributions applied for the real-data tomogram in Fig. 6. Note that the fast blocks have larger volume than the slow blocks. It is a mathematical property of relative residual tomography that the average of the velocity variations in a tomogram is zero. The volumes with zero velocity contrast in the input model will therefore tend to come out negative in the resulting tomogram.

Figure S3-3. As for Fig. S3-2, but for *S* velocity.

Figure S3-4. Recovery of variations in the V_P/V_S ratio. Because identical relative contrasts are used in V_P and V_S, we should get a zero anomaly in the V_P/V_S ratio. The low level of the recovered ratio quantifies the inversion noise level owing to differences in ray coverage in *S* and *P* arrivals.

(http://gji.oxfordjournals.org/lookup/suppl/doi:10.1093/gji/ggw370/-/DC1)